THERMAL-HYDRAULIC STUDIES IN SUPPORT OF THE ARIES-CS T-TUBE DIVERTOR DESIGN

S. I. ABDEL-KHALIK,*[a] L. CROSATTI,[a] D. L. SADOWSKI,[a] S. SHIN,[b] J. B. WEATHERS,[a] M. YODA,[a] and ARIES TEAM

[a]*George W. Woodruff School of Mechanical Engineering, Georgia Institute of Technology Atlanta, Georgia 30332-0405*
[b]*Hongik University, Department of Mechanical and System Design Engineering, Seoul 121-791, Korea*

Received April 16, 2007
Accepted for Publication August 2, 2007

This paper describes a numerical and experimental investigation in support of the ARIES-CS divertor design, which selected a modular, helium-cooled, T-tube design that can accommodate a peak heat load of 10 MW/m^2. Numerical analyses were carried out using the FLUENT computational fluid dynamics software package to evaluate the thermal performance of the divertor at the nominal design and operating conditions. Sensitivity studies were also performed to determine the effect of variations in geometry and operating conditions resulting from manufacturing tolerances and/or flow maldistribution between modules. The results indicate that the selected design is "robust" with respect to such anticipated variations in design and operational parameters and that a peak heat flux of 10 MW/m^2 can be accommodated within the constraints dictated by material properties. Extremely high heat transfer coefficients [>40 kW/(m^2·K)] were predicted by the numerical model; these values were judged to be "outside the experience base" for gas-cooled engineering systems. Hence, an experimental investigation was undertaken to verify the results of the numerical model. Variations of the local heat transfer coefficient within an air-cooled, geometrically similar test module were measured at the same Reynolds number as the actual helium-cooled divertor. Close agreement between the model predictions and experimental data was obtained. The results of this investigation provide added confidence in the results of the numerical model used to design the ARIES-CS divertor and its applicability to other gas-cooled high–heat flux components.

KEYWORDS: *magnetic fusion energy, stellarators, divertors*

Note: Some figures in this paper are in color only in the electronic version.

I. INTRODUCTION

The ARIES-CS study was launched with the goal of developing an attractive power plant concept based on the compact stellarator configuration through physics and engineering optimization. This paper focuses on the thermal-hydraulic analyses and experiments performed in support of the selected divertor design for ARIES-CS.

Divertors are used in magnetic fusion energy reactors to remove the fusion reaction ash (α particles), unburned fuel, and eroded particles from the reactor in order to maintain the quality of the plasma. The incident surface heat load distribution on the divertor depends on its surface topology, location, the reactor type, and plasma conditions; peak surface heat fluxes on the order of 10 MW/m^2 are expected. A significant fraction (~15%) of the total fusion thermal power is extracted by the divertor coolant. Several helium-cooled divertor concepts have been proposed[1–4]; their main advantages derive from their compatibility with a variety of blanket concepts and their ability to operate at high temperatures, which enhances the thermal efficiency of the power conversion systems.

The ARIES-CS conceptual design study considered a modular helium-cooled tungsten alloy divertor design accommodating a heat flux of up to 10 MW/m^2. Several designs were considered, including a tungsten plate design with a few large modules[2] and a modular "finger" configuration with jet impingement cooling from perforated endcaps, which requires a very large number of

*E-mail: said.abdelkhalik@me.gatech.edu

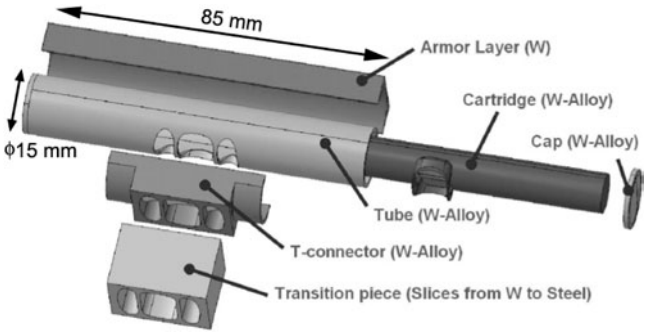

Fig. 1. T-tube divertor module geometry shown with component labels.[1]

small modules.[3,4] The T-tube modular design developed by Ihli et al.[1,3] was selected because it could accommodate the expected high heat fluxes using intermediate-size modules, thereby reducing the complexities associated with manufacturing and assembly of the much smaller modules of the finger design.[5] The concept is based on jet impingement cooling with a slot configuration.

The T-tube divertor module[1,3] is illustrated in Fig. 1. Helium at a flow rate per unit slot length of 0.4 kg/(s·m) enters the T-tube at 10 MPa and 873 K and exits at ~9.9 MPa and 953 K. For each T-tube divertor module, the coolant enters a concentric cartridge through an inlet port located midway along its length (Fig. 1). As shown in the cross section of Fig. 2 (right), this portion of the T-tube consists of two concentric tubes with a flat tungsten armor layer on top of the outer tube. Both tubes have capped ends and are separated by a 1.25-mm-wide annular gap. The inner tube (cartridge) has a narrow (0.5-mm-wide) slit along its entire length. For the nominal T-tube slit length of 8.5 cm, the total coolant mass flow rate is 0.034 kg/s. The coolant enters the inner tube and is accelerated through this slit toward the inner surface of the outer tube (Fig. 2). The stagnation point flow generated by the impingement of the nearly two-dimensional rectangular jet on this heated surface cools the divertor with a moderate pressure drop. Downstream of the stagnation location, the helium forms a turbulent wall jet along the inside surface of the outer tube and is then removed through the two exit ports near the center of the module (Fig. 1). Since stellarators should have no disruption events, the requirements on the armor layer are much less stringent than those for tokamaks. A flat armor layer with a minimum thickness of 0.3 mm was used in these studies (Fig. 1); an additional layer, however, can be brazed onto this basic armor if required.

Analyses have been performed to characterize the divertor geometry, location, and heat load distribution.[6] Detailed stress analysis of the T-tube divertor under its expected thermal and mechanical loads has been performed by Ihli et al.[1] This paper focuses on the numerical and experimental investigations of the thermal performance of the T-tube divertor design selected by the ARIES-CS team. Section II describes the numerical models used to analyze the divertor thermal performance. Section III presents the predictions from these numerical models at nominal design and operating conditions and the results of parametric studies performed to assess the sensitivity of the predicted performance to the selected turbulence model, along with variations in geometry and operating conditions resulting from manufacturing tolerances and/or flow maldistribution between modules. The experimental apparatus used to simulate the geometry and performance of the T-tube divertor module is described in Sec. IV. The section also compares the experimental data with the results of a priori numerical simulations performed with the same options used to model the actual T-tube divertor. Finally, Sec. V gives

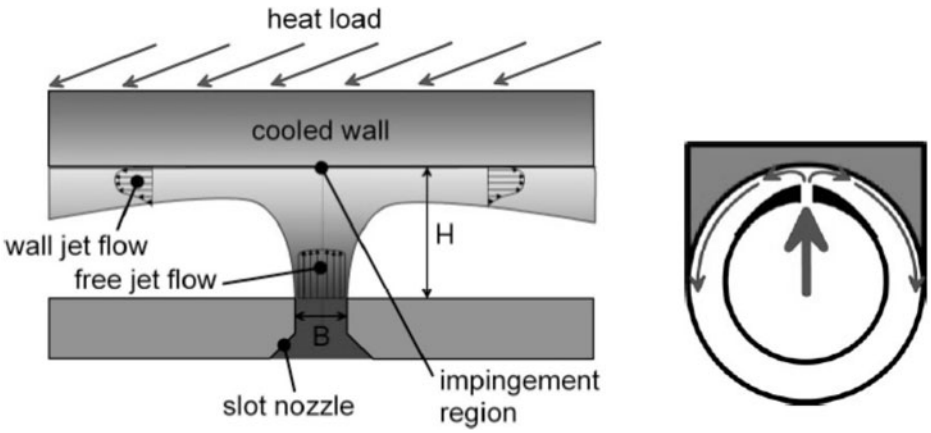

Fig. 2. Sketch of the impinging jet cooling method.[1] The reference value for the slot width $B = 0.5$ mm and for the annular gap $H = 1.25$ mm.

the conclusions and recommendations derived from this work.

II. NUMERICAL MODELS

Two-dimensional (2-D) and three-dimensional (3-D) analyses were performed using the FLUENT computational fluid dynamics (CFD) package to assess the thermal performance of the helium-cooled T-tube divertor at nominal design and operating conditions. Parametric analyses were also performed to assess the sensitivity of the predicted thermal performance to the selected turbulence-modeling options, as well as to changes in geometry and operating conditions due to manufacturing tolerances and/or flow maldistribution between modules. Figure 3 is a schematic of the 2-D model geometry, which represents a cross section of an infinitely long divertor module, and the corresponding mesh used in the numerical simulations. This 2-D model is used to examine the azimuthal variations in the heat transfer coefficient around the annular gap between the two concentric tubes. It is also used to explore the sensitivity of the divertor thermal performance to different types of turbulence models and variations in geometric parameters before carrying out the more computationally intensive 3-D analyses. Because of symmetry, the 2-D model represents only half the width of the divertor module, so the helium flow rate per unit slot length is only 0.2 kg/(s·m); i.e., only half the slot width is considered. The sizes of the inlet and exit ports in the 2-D model are selected to be considerably larger than the width of the inner tube slot to avoid distortions of the flow pattern as the coolant exits the inner tube and flows around the annular gap between the two

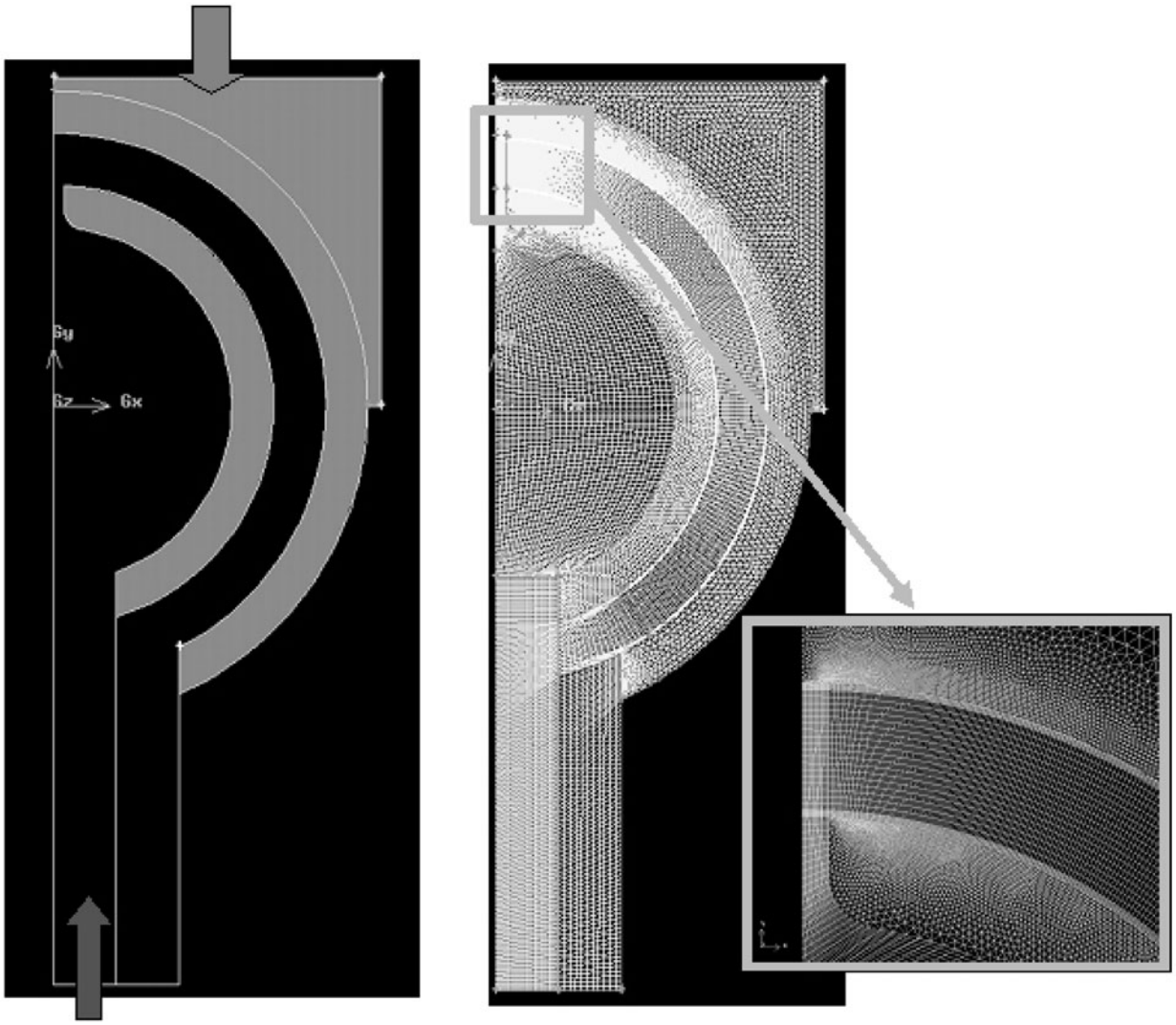

Fig. 3. 2-D model geometry and corresponding mesh used in the numerical simulations.

concentric tubes. An incident heat flux of 10 MW/m^2 is assumed at the plasma-facing tile surface. A volumetric heat generation rate of 53 MW/m^3 is also assumed in all tungsten structures based on results from the neutronic analysis.[7] The grid used in the numerical simulations for the 2-D model (Fig. 3) included nearly 36 000 cells; convergence studies confirmed that a finer grid had a negligible effect on the numerical predictions.

Figure 4 shows the 3-D model geometry and the corresponding mesh used in the simulations. The model, which represents only one-quarter of the actual T-tube divertor module because of symmetry in both the axial and vertical directions, is used to predict the actual performance of the T-tube divertor. As mentioned previously, the 3-D model is also used for selected parametric studies on how different types of turbulence models and variations in geometric parameters affect the results. Because of symmetry along the vertical plane (midway across the inner tube slot), the helium flow rate per unit slot length is again only 0.2 kg/(s·m). The incident heat flux at the plasma-facing surface and the volumetric heat generation in tungsten structures are assumed to be the same as those for the 2-D model. The grid used in the numerical simulations for the 3-D model (Fig. 4) included nearly 707 000 cells; convergence studies again confirmed that a finer grid had a negligible effect on the numerical predictions.

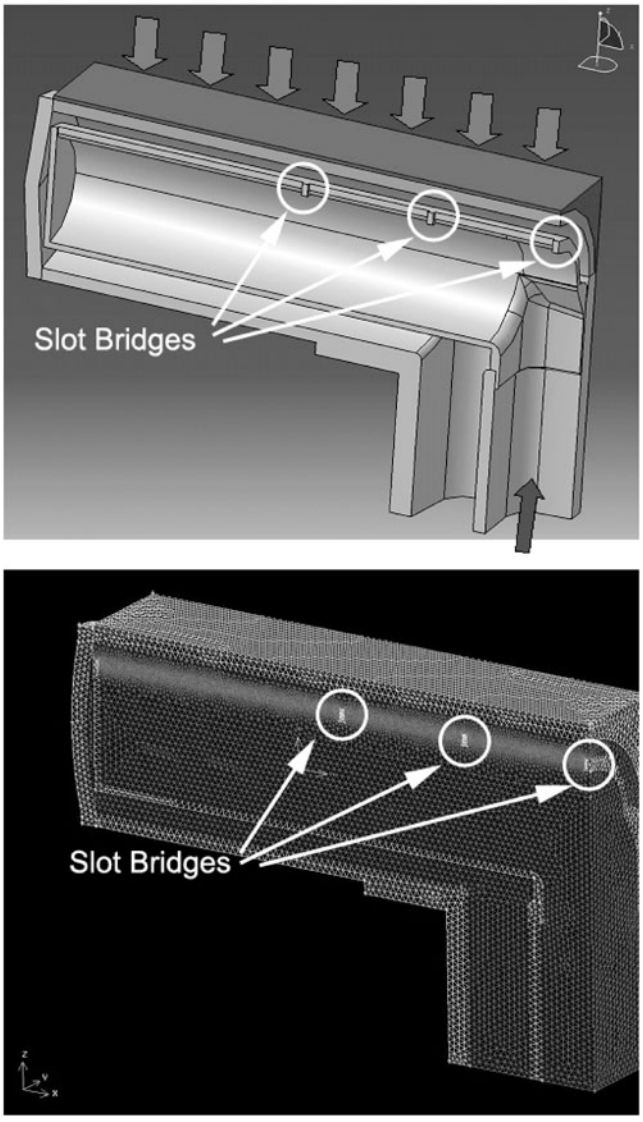

Fig. 4. 3-D model geometry and the corresponding mesh used in the simulations.

For both the 2-D and 3-D analyses, compressibility effects in the helium were modeled by the ideal-gas law, and the temperature dependence of the thermal conductivity and viscosity of helium and the thermal conductivity of tungsten were accounted for using equations based on fitted experimental data.[8] Property variations due to neutron irradiation have not been included. Parametric calculations were performed to quantify the effect of different turbulence models (namely, standard k-ε, realizable k-ε, and renormalized group, or RNG, k-ε) and additional options such as wall enhancement and nonequilibrium wall function available in FLUENT on the predicted temperature distribution and pressure drop. Calculations were also performed to examine the effect of variations in helium flow rate [0.4 kg/(s·m) ± 20%], helium exit pressure (10 MPa ± 10%), inner tube slot width (0.5 mm ± 20%), and annular gap thickness (1.25 mm ± 20%) on the numerical predictions. These calculations were aimed at assessing the "robustness" of the modular T-tube divertor design vis-à-vis expected changes in geometry and operating conditions resulting from manufacturing tolerances and/or flow maldistribution between modules.

III. NUMERICAL RESULTS

Table I summarizes the results of the parametric studies performed using the 2-D model. All analyses were performed using the FLUENT (V6.1) CFD software package. Referring to Table I, the results show that changing the turbulence model used in the analysis has a slight effect on the predicted maximum temperatures. For the nominal operating conditions with an incident heat flux of 10 MW/m^2, the predicted maximum temperature of the pressure boundary (outer tube-tile interface temperature) varies from 1525 K for the standard k-ε model to 1493 K for the RNG k-ε model; use of the standard k-ε model in the analyses may therefore yield slightly conservative maximum temperatures. In all cases, however, the maximum temperature of the pressure boundary is expected to be lower than the recrystallization temperature of the tungsten alloy used to manufacture the outer

TABLE I

Parametric Studies Performed Using the 2-D Model (Effects of Turbulence Model, Coolant Flow Rate, Exit Pressure, Slot Width, and Annular Gap Thickness)

	Maximum Tile Temperature (K)	Maximum Temperature of Tube/Tile Interface (K)	ΔP (kPa)
Standard k-ε, with wall enhancement model	1731	1525	55.75
Realizable k-ε, with wall enhancement model	1700	1504	47.38
Reference case (RNG k-ε with wall enhancement; mass flow rate = 0.4 kg/(s·m); P_{out} = 10 MPa; slot width = 0.5 mm; annular gap thickness = 1.25 mm)	1688	1493	46.83
Mass flow rate			
0.24 kg/(s·m)	1618	1423	66.34
0.16 kg/(s·m)	1788	1594	30.67
P_{out}			
9 MPa	1688	1493	52.06
11 MPa	1689	1493	42.56
Slot width			
0.4 mm	1633	1427	78.82
0.6 mm	1745	1563	31.23
Annular gap thickness			
1.0 mm	1695	1495	44.44
1.5 mm	1680	1491	49.69

tube[5] (~1573 K). The results in Table I also show that reduction of the coolant mass flow rate by nearly 20% may increase the peak temperature of the pressure boundary to its limit, whereas changes in the coolant inlet pressure by ±10% have an insignificant effect on the predicted peak temperatures. Clearly, the pressure drop values calculated using the 2-D model do not represent the pressure drop in the actual T-tube module because of the change in the coolant inlet and outlet flow configurations. Nevertheless, the trends in calculated pressure drop values for different inlet flow rates and coolant pressures are consistent with the expected behavior.

The results in Table I also show that changes in the annular gap thickness by ±20% (1.25 ± 0.25 mm) have a very minor effect (±2 K) on the predicted maximum temperatures. However, the predicted maximum temperatures are considerably more sensitive to changes in the inner tube slot width. A 20% reduction in the slot width (0.4 mm versus 0.5 mm) results in a lower peak temperature (1427 K versus 1493 K) and a significantly higher pressure drop. Hence, a system with multiple modules in parallel may cause the flow rate through the module with the narrower-than-normal slot to be significantly reduced from its nominal value of 0.4 kg/(m·s), which in turn may cause the peak temperature for such a module to be higher than that shown in Table I. For modules with a wider slot (0.6 mm versus 0.5 mm), the predicted maximum temperature will significantly increase (1563 K versus 1493 K) and the pressure drop will significantly decrease. This means that for multiple modules arranged in parallel, the flow rate through the module with the wider-than-normal slot will be higher than its nominal value, which in turn means that the peak temperature of the pressure boundary will be lower than the value shown in Table I.

Parametric calculations similar to those described above have been performed using the 3-D model (Table II). While the maximum temperatures predicted using the 3-D model are slightly different from those predicted using the 2-D model, the results indicate that for an incident heat flux of 10 MW/m^2, the maximum temperature of the tungsten alloy pressure boundary at the nominal design and operating conditions will be less than the recrystallization temperature (1573 K). The results also indicate that including wall enhancement and nonequilibrium wall function in the turbulence model used in the analysis will modestly impact the predicted maximum wall temperatures. The effects of coolant flow rate, coolant pressure, slot width, and annular gap thickness on the peak temperatures are similar to those described for the 2-D model. These results point to the "robustness" of the design with respect to changes in geometry resulting from manufacturing and assembly of the various modules.

TABLE II

Parametric Studies Performed Using the 3-D Model (Effects of Turbulence Model, Coolant Flow Rate, Inlet Pressure, Slot Width, and Annular Gap Thickness)

	Maximum Tile Temperature (K)	Maximum Temperature of Tube/Tile Interface (K)	ΔP (Pa)
3-D reference (standard k-ε, with wall enhancement; mass flow rate = 0.4 kg/(s·m); P_{out} = 10 MPa; slot width = 0.5 mm; annular gap thickness = 1.25 mm)	1699	1523	1.06×10^5
RNG k-ε, with wall enhancement	1726	1583	1.12×10^5
Standard k-ε			
Without wall enhancement	1723	1558	1.22×10^5
With nonequilibrium wall function	1762	1587	1.07×10^5
Mass flow rate			
3.3 kg/(s·m)	1782	1607	0.76×10^5
4.7 kg/(s·m)	1646	1466	1.55×10^5
P_{out}			
9 MPa	1701	1523	1.07×10^5
11 MPa	1719	1543	1.07×10^5
Slot width			
0.4 mm	1621	1452	1.67×10^5
0.6 mm	1720	1545	0.86×10^5
Annular gap thickness			
1.0 mm	1728	1557	0.89×10^5
1.5 mm	1716	1545	0.90×10^5

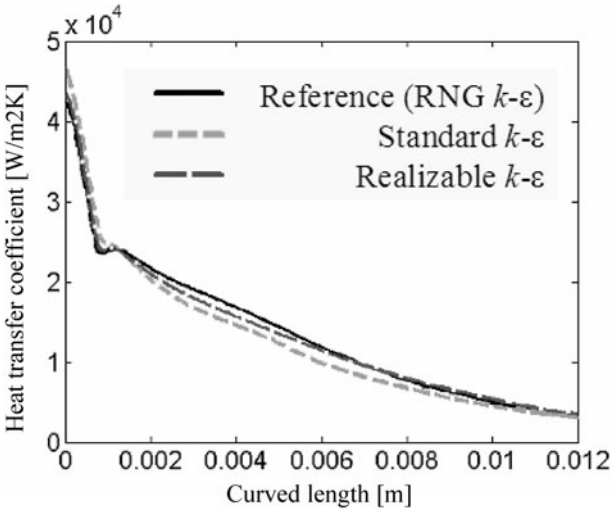

Fig. 5. Heat transfer coefficient versus position along the inner surface of the outer tube measured from the slit (2-D FLUENT simulations).[8]

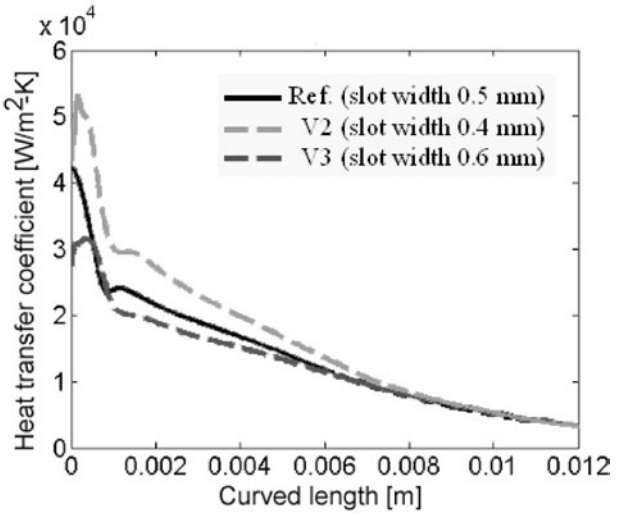

Fig. 6. Heat transfer coefficient versus position along the inner surface of the outer tube measured from the slit (2-D FLUENT simulations).[8]

Variations of the heat transfer coefficient around the annular gap predicted by the 2-D model are shown in Figs. 5 and 6. These results show that extremely high heat transfer coefficients are to be expected near the stagnation point as the jet issuing from the inner tube slit impacts the inner surface of the outer tube. The heat transfer coefficient gradually decreases as the coolant flows around the annular gap between the tubes. Figure 5

shows that the turbulence model to be selected has a modest effect on the predicted values for the heat transfer coefficient. On the other hand, Fig. 6 shows that for the same coolant mass flow rate, changes in the inner tube slot width will have a significant impact on the predicted heat transfer coefficients; considerably lower heat transfer coefficients are predicted as the slot width is increased, i.e., as the jet velocity issuing from the slot decreases. However, as indicated earlier, an increased slot width will lead to a lower module pressure drop, which in turn will lead to a higher-than-nominal coolant flow rate and higher heat transfer coefficients than those indicated in Fig. 6.

Examination of the results described above obtained using the FLUENT model show that the predicted heat transfer coefficient along the inner surface of the outer tungsten alloy tube is extremely high; values in excess of 40 kW/($m^2 \cdot K$) were obtained near the stagnation point immediately opposite to the inner tube slit (Figs. 5 and 6). Such values were judged to be "outside the experience base" for gas-cooled engineering systems since heat transfer coefficients on the order of 40 kW/($m^2 \cdot K$) are usually associated with nucleate boiling.[9] It was therefore deemed necessary to experimentally validate these results. To this end, an experimental investigation has been undertaken to validate the results of the numerical model. The aim is to design, construct, and instrument a test module that closely simulates the thermal-hydraulic behavior of the slot jet impingement heat transfer mechanism present in the helium-cooled T-tube divertor. Axial and azimuthal variations of the local heat transfer coefficients are measured over wide ranges of operating conditions. Calculations are performed a priori to predict the wall temperature distributions and heat transfer coefficients for the test module using the same methodology (i.e., FLUENT options) used to analyze the thermal performance of the actual T-tube divertor. The measured and predicted heat transfer coefficients are compared to assess the model's capabilities and validate its predictions.

IV. EXPERIMENTAL VALIDATION OF PREDICTED PERFORMANCE

IV.A. Experimental Test Section

The test section used to simulate the T-tube divertor module was designed to replicate the main feature of the T-tube divertor, the slot jet impingement heat transfer mechanism. Although the test section design accurately represents this aspect of the T-tube divertor module, it does not have uniform, one-sided heating or the exact divertor geometry of the T-tube design. The test section consists of two concentric tubes separated by an annular gap of 1.08 mm (Fig. 7). The inner diameter of the outer tube (14.86 mm) and the outer diameter of the inner tube (12.70 mm) are selected to nearly match those for the concentric tungsten alloy tubes of the T-tube divertor module, and the annular gap thickness (1.08 mm) is within the range of values (1.0 to 1.5 mm) considered in the parametric studies of the divertor thermal performance. The uniformity of the annular gap between the tubes is maintained over the total axial (z) extent of the outer tube (~220 mm) by placing three Teflon spacers at each end of the outer tube; each spacer has an azimuthal extent of about 60 deg (Fig. 8).

The 220-mm-long outer tube is made of 15.9-mm-o.d. Type 304 stainless steel tubing with a wall thickness of 0.51 mm. A 150-mm-long section of the outer tube centered along its 220-mm length is electrically heated

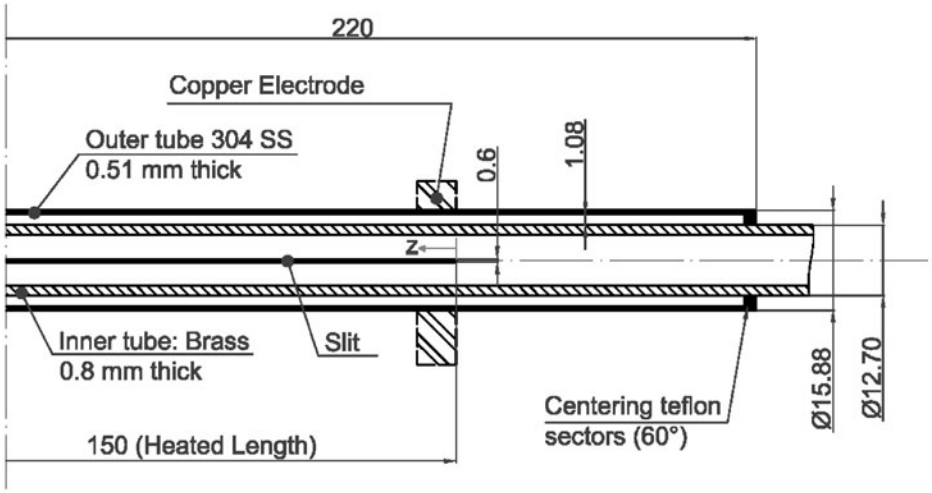

Fig. 7. Schematics of the test section showing the outer and inner tubes and the slit.

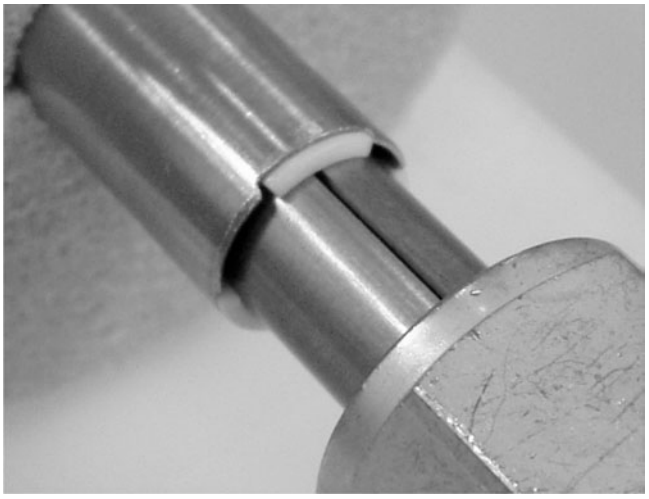

Fig. 8. Close-up photograph of the slit and Teflon sectors; the outer tube has been translated with respect to the inner tube.

by passing dc current through its wall via two copper electrodes clamped around the tube wall (Fig. 9) and connected to a dc power supply. The power input to the test section (i.e., the surface heat flux on the outer tube) is controlled by controlling the applied voltage between the electrodes. The power supply (Rapid Power Technologies, model 1198224) has an output range of 0 to 18 V and 0 to 2500 A, well in excess of the needed power input (75 to 300 W with a maximum current of 250 A). The power input is determined from the measured current and voltage drop; the current is measured using a calibrated 300-A shunt (Deltec Company MKB-600-100), and the voltage drop along the tube is measured using an Agilent data acquisition unit (model 34970 with A/D card 34901). Both the effective current and the effective voltage are measured using a four-wire method. The outer tube is thermally insulated using high-performance foam-pipe insulation.

The 12.7-mm-o.d. inner tube is made of brass with a wall thickness of 0.80 mm. The total length of the inner tube is 660 mm; a 0.60-mm-wide, 150-mm-long slit is cut through the tube wall. The slit is machined using a micromilling technique and is centered along the tube length to match the heated section of the outer tube. To prevent slit deformation due to residual stresses and ensure the uniformity of its width along the entire 150-mm length, two 1.2-mm-long (z direction) "slit bridges" were left uncut at equal axial intervals (50 mm) along its length. The slit bridges had a negligible effect on the temperature distribution and flow. Bored-through SWAGELOK heat exchanger fittings are used to maintain the axial position of the inner tube slit relative to the heated section of the outer tube, as well as the annular gap between tubes.

The outer surface of the outer tube is instrumented with nine self-adhesive thermocouples (Omega SA1-E,

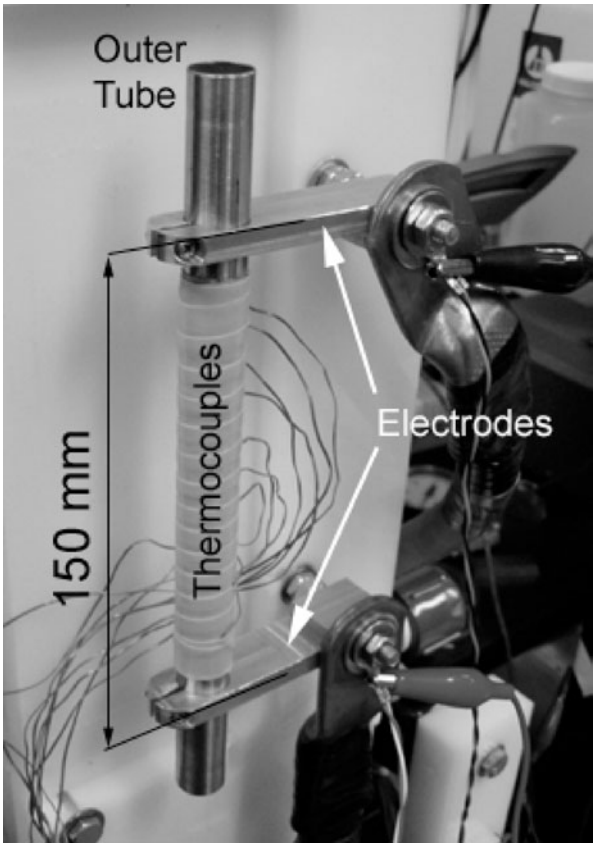

Fig. 9. Image showing the outer tube, electrodes, and nine thermocouples.

type E, Chromyl-Constantan). The thermocouple beads are located at axial locations 1 through 9, corresponding to axial positions z = 20.6, 34.2, 47.8, 61.4, 75, 88.6, 102.2, 115.8, and 129.4 mm (Fig. 10). All thermocouples are fixed to the surface at a specific azimuthal location. Since the bored-through fittings allow rotation of the outer tube relative to the inner tube, the nine thermocouples can be positioned at any azimuthal location relative to the inner tube discharge slit. Hence, detailed azimuthal variations of the outer tube surface temperature at the nine instrumented axial locations can be easily obtained by simply rotating the outer tube relative to the inner tube and repeating the experiment at the same operating conditions. Typically, data are obtained at 20-deg angular increments around the tube periphery. A scribe mark and an angular scale are used to indicate the azimuthal position θ of the thermocouple relative to centerline of the inner tube slit (Fig. 10). The azimuthal resolution of temperature measurement is limited by the size of the thermocouple beads and repeatability of the angular positioning; the estimated uncertainty in the azimuthal position of temperature measurement is less than 10 deg.

The data acquisition system consists of a 60-channel data acquisition unit (Agilent 34970A, with three A/D cards #34901A, 20 channels each), connected to a PC

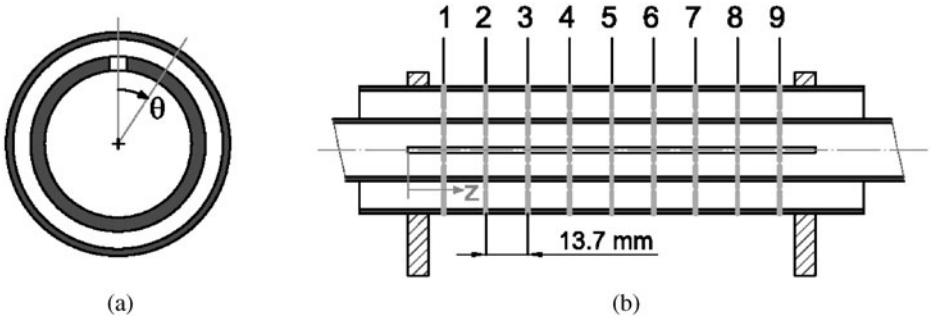

Fig. 10. Definition of (a) azimuthal coordinate θ and (b) axial coordinate z showing the thermocouple positions.

through an RS-232 serial cable. The Agilent Bench Link Data Logger 3 software package is used to configure the unit and monitor the data on the PC display. After steady state is reached, a Visual Basic code is used to configure the unit and control data acquisition. Only steady-state data are stored for each experiment.

IV.B. Experimental Flow Loop

Experimental studies are carried out by placing the test module described above in an air flow loop. The thermal-hydraulic behavior of the helium-cooled T-tube divertor module is closely simulated by performing experiments over a wide range of parameters spanning the expected range of nondimensional parameters for the actual divertor. Figure 11 shows the flow loop and test section used in these experiments. Air from a compressed-air line at a controlled pressure up to ~690 kPa [100 psi (absolute)] enters the flow loop and is discharged to the surroundings after flowing through the test module.

The inlet and exit pressures and mass flow rate through the test section are adjusted using needle valves at the inlet and outlet; the pressure at the outlet can be set at 1 atm by venting directly to the atmosphere. The mass flow rate through the test section is determined by measuring the volume flow rate and density (i.e., temperature and pressure) at the inlet and outlet. Multiple flow meters with different calibration ranges are used to ensure accurate

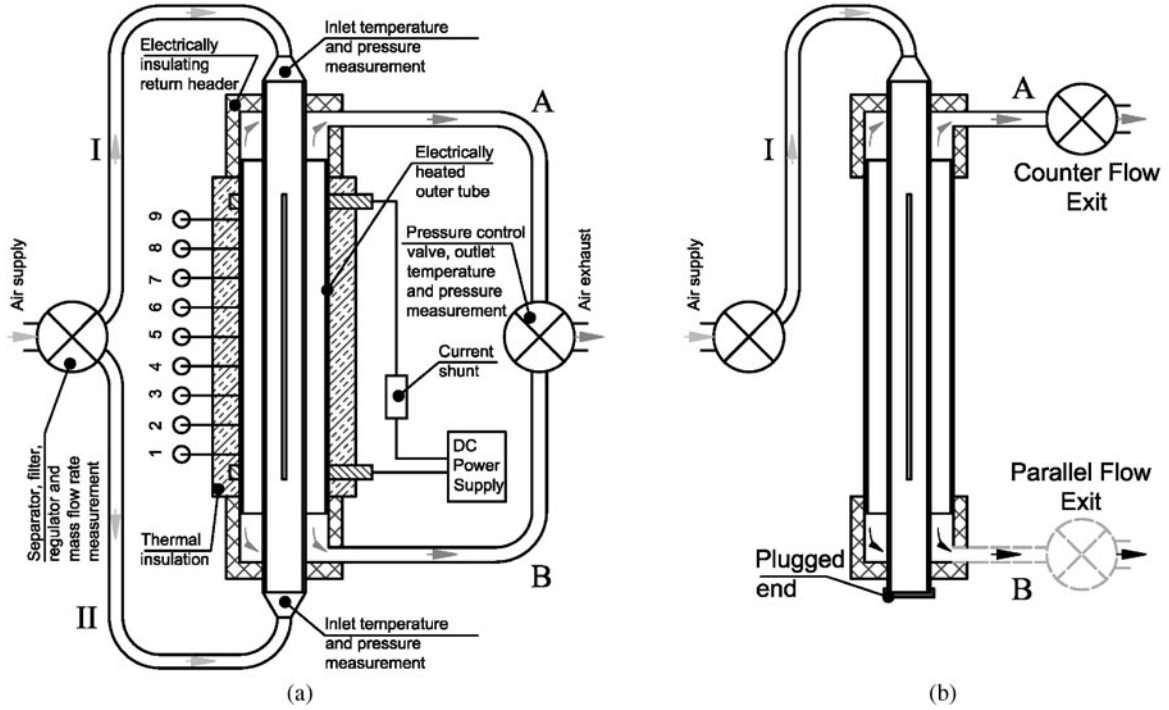

Fig. 11. Schematic of the experimental flow loop detailing the flow paths and instrumentation. (a) Double-inlet configuration and (b) counterflow and parallel flow configurations.

TABLE III

Comparison of Thermal-Hydraulic Parameters for the Proposed Helium-Cooled T-Tube Divertor and the Experimental Studies Using Air

Parameter	Air			Helium
	Low	Medium	High	
Operating pressure	100 kPa	300 kPa	600 kPa	10 MPa
Pressure drop	3.7 kPa	30 kPa	~200 kPa	0.1 MPa
Mass flow rate (per unit slit length)	27 g/(s·m)	100 g/(s·m)	180 g/(s·m)	400 g/(s·m)
Inlet temperature	20°C	20°C	20°C	600°C
Average Re	2.9×10^3	1.1×10^4	2.0×10^4	1.9×10^4
Pr	0.71	0.71	0.71	0.66

measurements over the entire parameter range used in the experiments. A Venturi flowmeter (Lambda Square CBV075) and a calibrated orifice flowmeter with an 0.800-cm-diameter orifice (Meriam S/N 647640-S1) are placed upstream of the test section, and a positive displacement gas flowmeter (Rockwell International R-315) is placed at the exit. The inlet and exit air temperatures are measured using E-type thermocouple probes (Omega EMQSS-062E-12). The inlet and exit gauge pressures and the differential pressure across the orifice are measured using differential pressure transducers with appropriate ranges (Omega PX26-xxxDV). The ambient pressure is measured using an absolute pressure transducer (Omega PX302-015AV) and a mercury barometer. An inclined manometer (Dwyer 244) is used to measure the pressure drop across the Venturi flowmeter.

The test conditions are selected to cover a broad range of parameters spanning the nondimensional parameter values for the actual helium-cooled divertor module. Since the geometry is nearly prototypical, the most important nondimensional parameter is the Reynolds number based on slit conditions. Table III compares the test conditions for three experiments with the flow conditions for the T-tube divertor. The Reynolds number based on the slit hydraulic diameter Re = 2.9×10^3 to 2.0×10^4; the value for the helium-cooled divertor at nominal operating conditions is 1.9×10^4. The difference between the Prandtl numbers for air (0.77) and helium (0.66) is judged to have a small effect on the measured Nusselt number. Regardless of its value, however, the aim of these experiments is to validate the FLUENT numerical model used to determine the thermal performance of the helium-cooled divertor. Should the model prove successful in matching the experimental data over the covered ranges on nondimensional parameters, one would gain confidence in its ability to correctly model the actual divertor performance.

IV.C. Flow Configurations

In addition to modeling the flow conditions within the T-tube divertor geometry, the flow loop (Fig. 11) was designed to examine other flow configurations while utilizing the same basic rectangular jet impingement cooling concept. Referring to Figs. 11 and 12, three different flow configurations can be examined:

1. *Double inlet*, in which the coolant enters the inner tube at both ends (I and II in Fig. 11a) and exits at both ends of the outer tube (A and B in Fig. 11a). Given the symmetry of this configuration, the flow will tend to "stagnate" near the center of the inner tube midway along the slit length.

2. *Counterflow*, in which the coolant enters the inner tube from only one end (e.g., at I in Fig. 11b) and exits the outer tube at A, i.e., the same end. In this configuration, a fluid particle must exit at the same end as it entered, resulting in significantly reduced velocities near the opposite end.

3. *Parallel flow*, in which the coolant enters the inner tube from only one end (e.g., at I in Fig. 11b) and exits the outer tube at B, i.e., the opposite end. A fluid particle in this configuration must traverse the entire axial extent

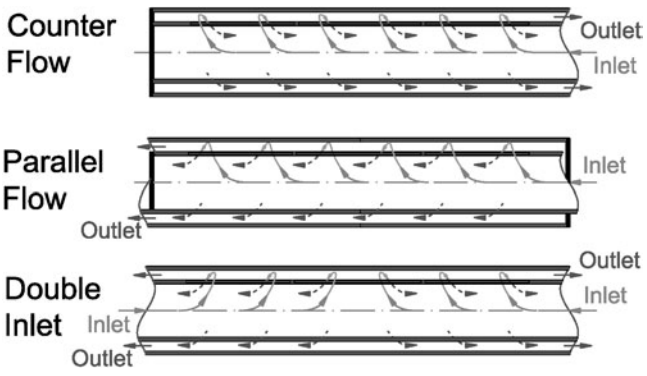

Fig. 12. Flow visualizations for counterflow, parallel flow, and double-inlet flow configurations

of the test section before exiting, resulting in a fairly uniform flow along the length of the test section.

Experiments were conducted using all three flow configurations.

IV.D. Numerical Simulation of Experiments

As indicated earlier, a priori numerical simulations were performed to predict the wall temperature distributions and heat transfer coefficients for the experimental test module geometry and conditions using the same methodology (i.e., FLUENT code options) used to analyze the thermal performance of the actual helium-cooled T-tube divertor (Secs. II and III). This section describes the method used to perform these a priori numerical simulations; comparisons between the predicted and measured heat transfer coefficients for several typical experiments are presented in Sec. IV.E.

Depending on the flow configuration to be used in an experiment (Fig. 12), either a quarter- or half-model geometry was used in the numerical simulations (Fig. 13). The model included the two concentric tubes, the surrounding insulation, the electrodes connected to the outer tube, fittings, and mounting brackets. Including these components in the model ensures an accurate energy balance consistent with the measurements. The boundary conditions used in the simulations specify the power input to the outer tube, coolant (air) mass flow rate, exit pressure, and heat transfer coefficient between the test module (i.e., outer insulation surface) and the ambient; the latter is based on estimates made using natural convection correlations from vertical cylinders, and all other parameters correspond to their respective measured values for each experiment to be analyzed.

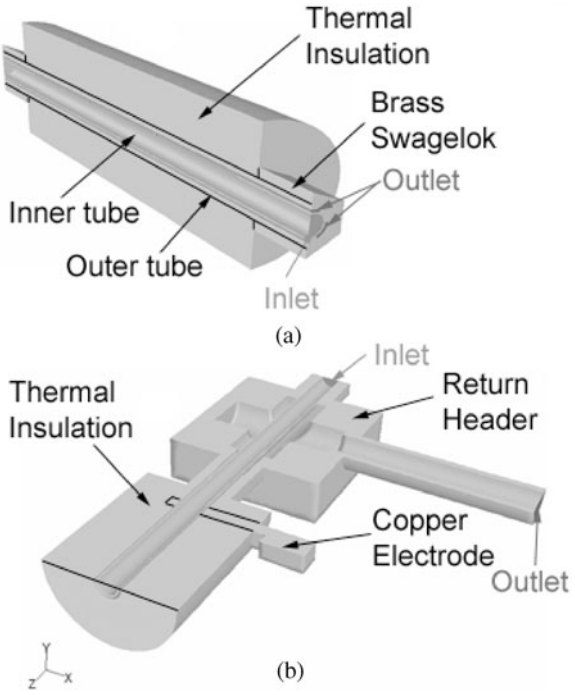

Fig. 13. (a) Typical half-model in counter/parallel flow configuration showing the tube surrounded by insulating foam and (b) typical quarter-model in double-inlet configuration showing foam, mounting brackets, and electrodes.

Simulations are carried out using computational grids with up to 10^6 cells (Fig. 14). Grid convergence studies with double, 1.2 times, and 1.3 times the axial, tangential, and radial resolutions, respectively, indicated that the numerical predictions had converged for all cases shown here. In most cases, the CFD solutions converged within 5 h on a Pentium IV 3.4-GHz workstation with 2-GB RAM. Comparisons between the results of the numerical simulations and the experimental data are given in the following section.

IV.E. Comparison Between Experimental Data and Model Predictions

In this section, the experimental data are compared with the predictions of the FLUENT model described above. Figure 15 shows the experimental and numerical azimuthal temperature profiles for the outer tube surface at two axial locations, 2 (closed triangles) and 8 (closed circles), which are symmetrically located along the inner tube slit length (Fig. 10), for the double-inlet flow configuration at an average Reynolds number $\mathrm{Re} = 1.1 \times 10^4$, or medium flow conditions (Table I). The solid and dashed lines denote FLUENT results obtained using standard and RNG k-ε models, respectively. The error bars in the angular position θ represent positioning errors (cf. Sec. IV.A), whereas those in the temperature T represent the standard deviation in the estimated measurement errors averaged over the two symmetric azimuthal locations with respect to the slit (e.g., $\theta = 20$ and 340 deg). The agreement between the experimental profiles at the two axial thermocouple locations suggests that, as expected, the flow in the test section is symmetric about the slit midpoint, i.e., the stagnation plane at $z = 75$ mm (axial location 5 in Fig. 10). The maximum temperature occurs at the stagnation point opposite the slit ($\theta = 180$ deg) where the two opposed wall jets flowing along the inner surface of the outer tube meet. As indicated earlier, the FLUENT results are essentially identical for the two different turbulence models; therefore, only the results obtained using the standard k-ε model are shown.

Clearly, Fig. 15 shows good agreement between the measured and predicted temperatures of the outer tube (i.e., heated surface). One therefore would expect the azimuthal variations of the local heat transfer coefficient at these two axial locations to be also in agreement, as can be seen in Fig. 16. It should be noted, however, that even though the outer tube wall is uniformly heated both axially and azimuthally by the applied dc current, the

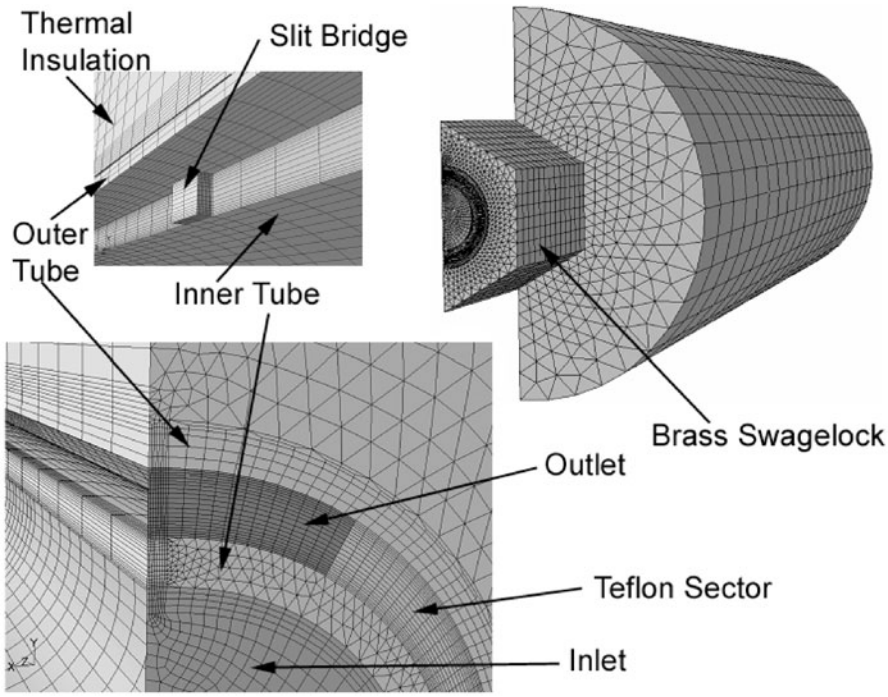

Fig. 14. Typical computational grids used in numerical simulations of the experimental test section

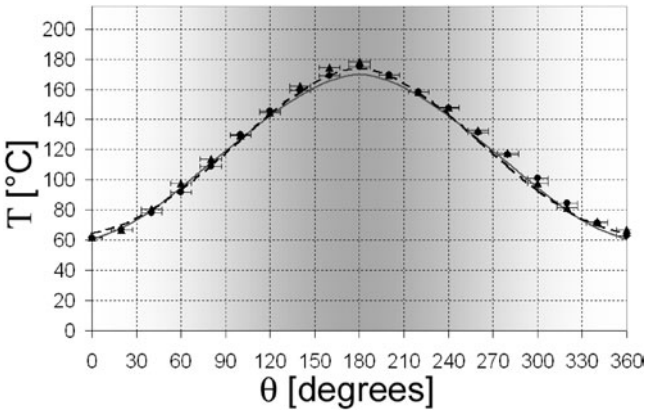

Fig. 15. Experimental and numerical results for $T(\theta)$ at thermocouple locations 2 (triangles) and 8 (circles), which are symmetrically located along the inner tube slit length (double inlet, Re = 1.1×10^4).

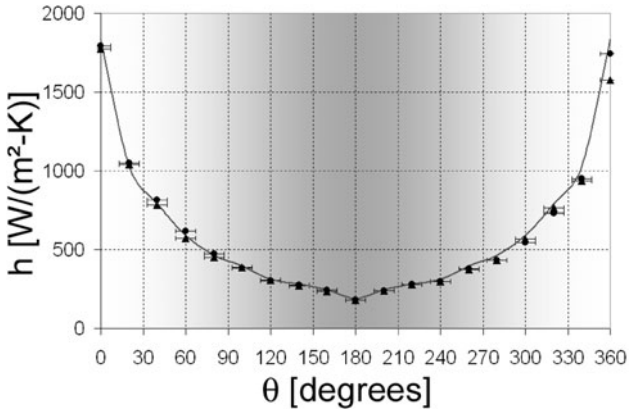

Fig. 16. Experimental and numerical results for $h(\theta)$ at thermocouple locations 2 and 8 (double inlet, Re = 1.1×10^4).

heat flux at the inner surface may not be uniform because of axial and azimuthal conduction through the tube wall. Since the local heat flux is not directly measured, the calculated values of the local heat flux are used in conjunction with the measured wall temperatures to determine the experimental heat transfer coefficients:

$$h_{exp} = \frac{q''_{\mathrm{CFD}}}{T_w - T_{in}} \ ,$$

where T_w is the measured local wall temperature and T_{in} is the coolant inlet temperature.

Figure 16 shows good agreement between the experimental and predicted values of the local heat transfer coefficients. The peak values of the local heat transfer coefficients occur at the stagnation point ($\theta = 0$ and 360 deg), where the rectangular jet issuing from the inner tube slit impacts the inner surface of the outer tube (Fig. 10a). It should be noted that the peak values in Fig. 16 [$\sim$1.7 kW/(m$^2 \cdot$K)] are well below the calculated

peak values for the actual helium-cooled T-tube divertor [$\sim$40 kW/(m$^2\cdot$K)]; this is to be expected since the thermal conductivity of helium at 100 bar and 600 K is more than an order of magnitude higher than that for air at 3 bar and 300 K. In other words, at a given local Nusselt number, a helium-cooled system will give a significantly higher heat transfer coefficient than the air-cooled system with the same geometry and Reynolds number. The Nusselt number corresponding to the peak heat transfer coefficient in Fig. 16 [$\sim$1.7 kW/(m$^2\cdot$K)] is 40.3 (characteristic length is the slot width).

Figure 17 shows axial variations (z profiles) in the experimental and predicted values of the local heat transfer coefficient for the same experiment described above (double-inlet flow configuration at Re = 1.1×10^4). Values of the heat transfer coefficients at all nine instrumented axial locations (Fig. 10b) are shown for $\theta = 0$ deg (squares), 20 deg (diamonds), 60 deg (triangles), 120 deg (circles), and 180 deg (squares). The lines denote the values predicted by the FLUENT model, and the symbols denote the experimental values. As expected for this double-inlet flow configuration, the heat transfer coefficient reaches a minimum near the midway plane along the inner tube slit (thermocouple location 5). For a given axial location, the heat transfer coefficient decreases as the two wall jets proceed azimuthally away from the stagnation point, where the jet issuing from the inner tube slit impacts the inner surface of the outer tube (θ = 0 deg). For θ values greater than about 20 deg, the heat transfer coefficient is essentially independent of axial location.

Results similar to those shown in Figs. 15, 16, and 17 for the parallel flow arrangement (Fig. 12) at Re = 1.1×10^4, or medium flow conditions, are shown in Figs. 18, 19, and 20, respectively. Again, these results show good

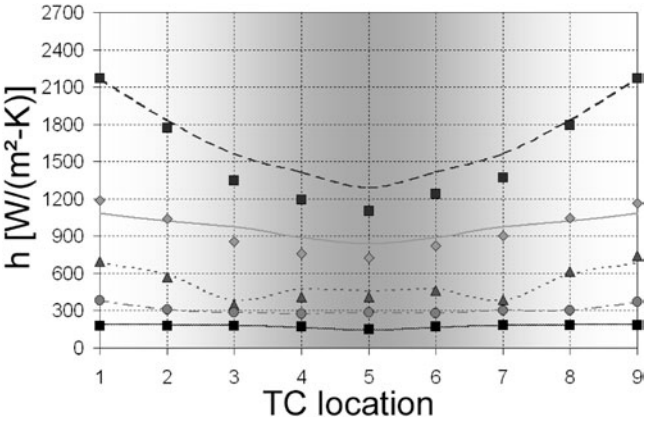

Fig. 17. Axial distribution of the heat transfer coefficient at instrumented thermocouple locations for $\theta = 0$ deg (squares), 20 deg (diamonds), 60 deg (triangles), 120 deg (circles), and 180 deg (squares) (double inlet, Re = 1.1×10^4).

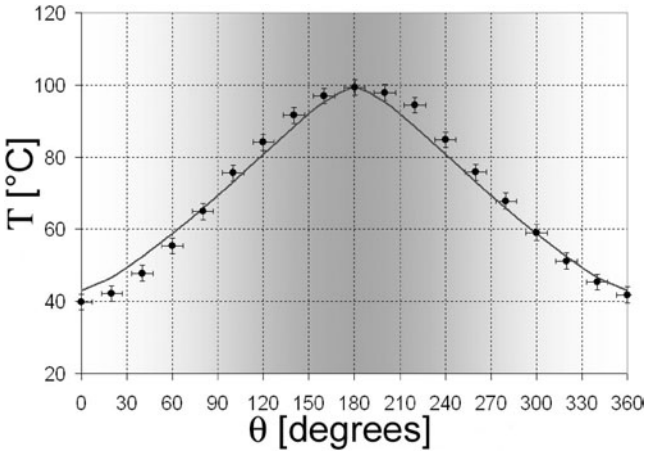

Fig. 18. Experimental (circles) and numerical (line) results for $T(\theta)$ at thermocouple location 3 (parallel flow, Re = 1.1×10^4).

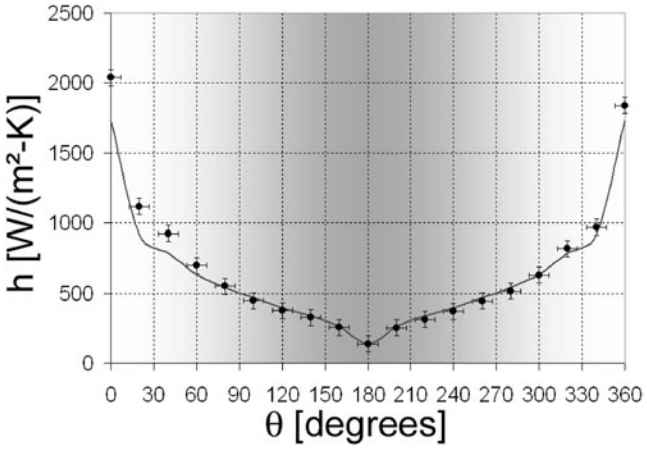

Fig. 19. Experimental (circles) and numerical (line) results for $h(\theta)$ at thermocouple location 3 (parallel flow, Re = 1.1×10^4).

agreement between the experimental data and model predictions. In all cases, the difference between the experimental and predicted values of the heat transfer coefficient is $<$20%. It should be noted that the axial variations in heat transfer coefficient shown in Figs. 17 and 20 can assist the designer in selecting an optimal module length (and flow configuration) to avoid significant degradation in the local heat transfer coefficient.

V. CONCLUSIONS AND RECOMMENDATIONS

This work describes the numerical and experimental studies of the modular helium-cooled T-tube divertor design performed as part of the ARIES compact stellarator

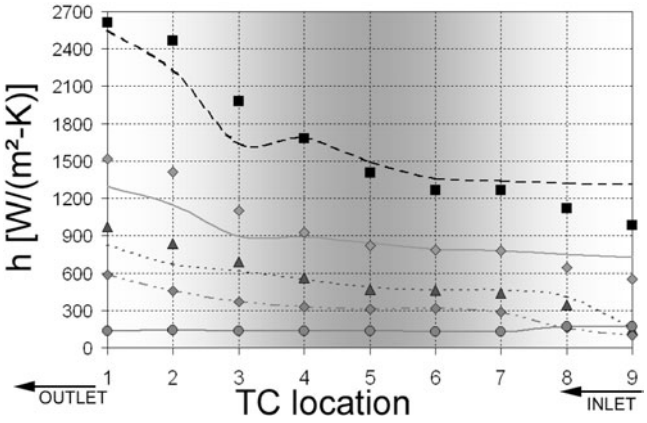

Fig. 20. Axial distribution of the heat transfer coefficient at instrumented thermocouple locations for $\theta = 0$ deg (squares), 20 deg (diamonds), 60 deg (triangles), 120 deg (diamonds), and 180 deg (circles) (parallel flow, $\mathrm{Re} = 1.1 \times 10^4$).

study. The experimental studies were motivated by the need to verify the numerical results that predicted heat transfer coefficients in excess of 40 $\mathrm{kW/(m^2 \cdot K)}$. Axial and azimuthal profiles of the local heat transfer coefficient were measured in an air-cooled test module that closely simulates the actual T-tube divertor module geometry and the thermal-hydraulics of rectangular jet impingement cooling. Experiments were carried out over a wide range of parameters encompassing the expected nondimensional parameter range for the helium-cooled T-tube divertor. A priori numerical simulations were performed to predict the temperature distributions and heat transfer coefficients for the experimental test module geometry and conditions using the same methodology (i.e., FLUENT code options) used to analyze the thermal performance of the actual helium-cooled T-tube divertor. Although the test module geometry does not exactly duplicate that of the T-tube divertor (e.g., uniform heating versus one-sided heating), the main feature affecting heat removal in the T-tube divertor, namely, impingement of the coolant jet issuing from the slit onto the inner surface of the outer cylinder followed by tangential flow in the annular region between the two cylinders, has been replicated. By validating the code predictions for the thermal performance of the test module against experimental data, strong inference can be made regarding the code's ability to correctly model the thermal performance of the actual T-tube divertor module geometry at the same thermal-hydraulic conditions (i.e., Reynolds number).

The model predictions are in good agreement with the experimental data, thereby providing confidence in the predicted performance of the ARIES-CS helium-cooled T-tube divertor design. Specifically, the divertor can accommodate an incident heat flux of up to 10 $\mathrm{MW/m^2}$ and is "robust" with respect to anticipated changes in geometry and operating conditions resulting from manufacturing tolerances and/or flow maldistribution among the modules.[8] The results also suggest that commercially available CFD software such as FLUENT can be confidently used to predict the thermal performance of similar helium-cooled divertors.

ACKNOWLEDGMENTS

This work has been performed as a part of the ARIES-CS study. We thank the U.S. Department of Energy Office of Fusion Energy Sciences for its support through contract DE-FG02-01ER54656.

REFERENCES

1. T. IHLI, A. R. RAFFRAY, and ARIES TEAM, "ARIES CS Report: Helium Cooled Divertor Design Study," UCSD-CER-06-04 (2005); http://aries.ucsd.edu/CER/reports.shtml.

2. S. HERMSMEYER and S. MALANG, "Gas-Cooled High Performance Divertor for a Power Plant," *Fusion Eng. Des.*, **61–62**, 197 (2002).

3. T. IHLI et al., "Gas-Cooled Divertor Design Approach for ARIES-CS," *Proc. 21st IEEE/NPSS Symp. Fusion Engineering (SOFE)*, Knoxville, Tennessee, September 26–29, 2005.

4. P. NORAJITRA et al., "State of the Art: Development of a Helium-Cooled Divertor for Demo," *Proc. 30th Symp. Fusion Engineering (SOFE)*, San Diego, California, October 14–17, 2003.

5. T. IHLI, A. R. RAFFRAY, S. I. ABDEL-KHALIK, S. SHIN, and ARIES TEAM, "Design and Performance Study of the Helium-Cooled T-Tube Divertor Concept," *Fusion Eng. Des.*, **82**, 249 (2007).

6. T. K. MAU et al., "Divertor Configuration and Heat Load Assessment for ARIES-CS," presented at ARIES Mtg., Princeton, New Jersey, October 4–5, 2006; http://aries.ucsd.edu/ARIES/MEETINGS/0610/Mau_divertor.pdf.

7. L. EL-GUEBALY et al., "Benefits of Radial Build Minimization and Requirements Imposed on ARIES Compact Stellarator Design," *Fusion Sci. Technol.*, **47**, 432 (2005).

8. S. SHIN et al., "Thermal Analysis of Helium-Cooled T-Tube Divertor," ARIES Project Presentation, Madison, Wisconsin, June 14–15, 2005; http://aries.ucsd.edu/ARIES/MEETINGS/0506/Abdel-Khalik.pdf.

9. F. P. INCROPERA and D. P. DeWITT, *Fundamentals of Heat and Mass Transfer*, 5th ed., p. 8, John Wiley & Sons, New York (2002).